

multistep working stroke found here is a common feature of the mechanism of force production by myosin motors, or whether it is a peculiar feature of the myosin-I used in this study. □

Methods

Protein preparations and solutions. Rat liver myosin-I (130K, the myr-1a gene product) and chicken brush-border myosin-I were isolated by gel filtration, anion and cation exchange chromatography as described^{7,13}. Rabbit skeletal-muscle myosin S1, rhodamine-phalloidin-labelled F-actin and N-ethyl maleimide (NEM)-modified myosin were also prepared by standard methods^{20,21}.

We used an optical tweezers transducer that is built around a Zeiss Axiovert microscope⁶. Experiments were performed within a 'flow-cell' made from a microscope slide and pieces of coverslip. Glass microspheres (1.7 μm) were applied to the coverslip surface as a suspension in 0.1% w/v nitrocellulose/amyl acetate. After drying this was made into a 0.1-mm-deep flow-cell and either BBM-1, myr-1 or skeletal S1 was allowed to bind to the coverslip surface using 0.2, 0.2 and 1 μg ml⁻¹ of protein, respectively, in a buffered salt solution²¹ (containing in mM: 25 KCl, 25 imidazole, 4 MgCl₂, 1 EGTA, pH 7.4, 23 °C). The solution was replaced with one containing rhodamine-phalloidin-labelled actin filaments and 1.1 μm polystyrene beads which were pre-coated with NEM-modified myosin (and the buffered salt solution was supplemented with, in mM: 2 creatine phosphate, 20 dithiothreitol (DTT), 0.01 to 0.1 ATP; and in mg ml⁻¹: 1 creatine phosphokinase, 0.5 BSA, 3 glucose, 0.1 glucose oxidase, 0.02 catalase²²). A single actin filament was captured between two polystyrene beads held suspended in mid-solution in two independent optical tweezers^{23,6} in the vicinity of the stationary glass microsphere. Its interaction with the surface-bound myosin was monitored by casting the image of one of the latex beads onto a 4-quadrant photo-detector. With the actin filament held taut but in the absence of myosin binding, the r.m.s. amplitude of brownian motion is given by $(kT/2\kappa_{\text{trap}})^{0.5} \sim 8.5 \text{ nm}$ r.m.s. (where kT = thermal energy; κ_{trap} = optical tweezer stiffness = 0.028 pN nm⁻¹). When myosin binds to the actin filament the beads are restrained by an additional stiffness (κ_{add}) which reduces the r.m.s. amplitude of their motion to $(kT/(2\kappa_{\text{trap}} + \kappa_{\text{add}}))^{0.5}$. Brownian motion shows a lorentzian power-density distribution with a roll-off frequency $f_c = \kappa/2\pi\beta \sim 430 \text{ Hz}$ (where $\beta = 6\pi\eta r$; η = solution viscosity, r = bead radius = 0.55 μm).

To improve the time resolution with which the onset of attachments could be detected we oscillated the position of one laser tweezer (at a frequency of $f = 1 \text{ kHz}$ and r.m.s. amplitude, $A_0 = 90 \text{ nm}$) and monitored transmission of this motion to the other bead. The combined effect of viscous damping and series elastic elements⁹ caused the amplitude of the resultant right-hand-side bead movement to be much smaller and to drop dramatically upon myosin binding ($A_r \approx (A_0\kappa_{\text{trap}})/(\kappa_{\text{tot}}^2 + (2\beta 2\pi f)^2)^{0.5}$; where $\kappa_{\text{tot}} = 2\kappa_{\text{trap}} + \kappa_{\text{add}}$ and during myosin attachment κ_{add} increases from zero to about 0.4 pN nm⁻¹). By oscillating the optical tweezer in this way it was possible to identify the start and end of each skeletal muscle myosin attachment from the r.m.s. amplitude of the 1 kHz sine wave with a time resolution of ~1 ms.

To ensure that the records we obtained derive from single myosin heads, we first made measurements at high surface densities of myosin and found that the actin filament was translated by several hundred nanometres, often pulling the beads completely out of the optical tweezers, under these conditions the bound lifetime was very non-linear with [ATP]. Then the myosin surface density was adjusted by diluting the myosin-containing solution such that single isolated events with long intervening periods of free bead diffusion were observed. At this surface density of myosin, about half of the stationary beads tested showed no interactions with the actin filament (we could find no active myosin on any region of the bead). Electron micrographs (not shown) showed that both myr-1 and BBM-1 deposited as monomers on nitrocellulose and did not clump or dimerize on the surface. Furthermore, the single extra step observed in the myosin-I records could be readily identified in about 80% of the events. Stiffness of the optical tweezers (κ_{trap}) was calibrated by applying a large amplitude triangular waveform displacement to the microscope stage (stage velocity, v) and by measuring the resulting bead displacement (d) caused by viscous drag force; giving $\kappa_{\text{trap}} = \beta v/d$. The 4-quadrant photodetector was calibrated by moving the trapped bead by a known amount using the laser beam steering devices. The bandwidth of the 4-quadrant photodetector was

5 kHz. Data were sampled at 10 kHz, digitized to 12 bits and stored on computer disk.

Received 21 December 1998; accepted 11 February 1999.

- Huxley, H. E. The mechanism of muscular contraction. *Science* **164**, 1356–1366 (1969).
- Huxley, A. F. & Simmons, R. M. Proposed mechanism of force generation in striated muscle. *Nature* **233**, 533–538 (1971).
- Jontes, J. D., Wilson-Kubalek, E. M. & Milligan, R. A. A 32° tail swing in brush border myosin-I on ADP release. *Nature* **378**, 751–753 (1995).
- Whittaker, M. et al. A 35 Å movement of smooth muscle myosin on ADP release. *Nature* **378**, 748–751 (1995).
- Irving, M. et al. Tilting of the light-chain region of myosin during step length changes and active force generation in skeletal muscle. *Nature* **375**, 688–691 (1995).
- Molloy, J. E., Burns, J. E., Kendrick-Jones, J., Tregear, R. T. & White, D. C. S. Movement and force produced by a single myosin head. *Nature* **378**, 209–212 (1995).
- Coluccio, L. M. & Conaty, C. Myosin-I in mammalian liver. *Cell Motil. Cytoskel.* **24**, 189–199 (1993).
- Coluccio, L. M. Differential calmodulin binding to three myosin-I isoforms from liver. *J. Cell. Sci.* **107**, 2279–2284 (1994).
- Veigel, C., Bartoo, M. L., White, D. C. S., Sparrow, J. C. & Molloy, J. E. The stiffness of rabbit skeletal, acto-myosin cross-bridges determined with an optical tweezers transducer. *Biophys. J.* **75**, 1424–1438 (1998).
- White, H. D. & Taylor, E. W. Energetics and mechanism of actomyosin adenosine triphosphatase. *Biochemistry* **15**, 5818–5826 (1976).
- Molloy, J. E., Kyrtatas, V., Sparrow, J. C. & White, D. C. S. Kinetics of flight muscles from insects with different wingbeat frequencies. *Nature* **328**, 449–451 (1987).
- Suzuki, Y., Yasunaga, T., Ohkura, R., Wakabayashi, T. & Sutoh, K. Swing of the lever arm of a myosin motor at the isomerization and phosphate release steps. *Nature* **396**, 380–383 (1998).
- Jontes, J. D., Milligan, R. A., Pollard, T. D. & Ostap, M. Kinetic characterization of brush border myosin-I ATPase. *Proc. Natl Acad. Sci. USA* **94**, 14332–14337 (1997).
- Williams, R. & Coluccio, L. M. Novel 130kDa rat liver myosin-I will translocate actin filaments. *Cell Motil. Cytoskel.* **27**, 41–48 (1994).
- Collins, K., Sellers, J. R. & Matsudaira, P. Calmodulin dissociation regulates brush border myosin-I (110kDa-calmodulin) mechanochemical activity. *J. Cell Biol.* **110**, 1137–1147 (1990).
- Toyoshima, Y. Y. et al. Myosin subfragment-1 is sufficient to move actin filaments *in vitro*. *Nature* **328**, 536–539 (1987).
- Iwane, A. H., Kitamura, K., Tokunaga, M. & Yanagida, T. Myosin subfragment-1 is fully equipped with factors essential for motor function. *Biochem. Biophys. Res. Commun.* **230**, 76–80 (1997).
- Howard, J. Molecular motors: structural adaptations to cellular functions. *Nature* **389**, 561–567 (1997).
- Jontes, J. D. & Milligan, R. A. Brush border myosin-I structure and ADP-dependent conformational changes revealed by cryoelectron microscopy and image analysis. *J. Cell Biol.* **139**, 683–693 (1997).
- Molloy, J. E. et al. Single molecule mechanics of heavy meromyosin and S1 interacting with rabbit or *Drosophila* actins using optical tweezers. *Biophys. J.* **68**, 2988–3055 (1995).
- Kron, S. J. & Spudich, J. A. Fluorescent actin filaments move on myosin fixed to a glass surface. *Proc. Natl Acad. Sci. USA* **83**, 6272–6276 (1986).
- Kishino, A. & Yanagida, T. Force measurements by micromanipulation of a single actin filament by glass needles. *Nature* **334**, 74–76 (1988).
- Finer, J. T., Simmons, R. M. & Spudich, J. A. Single myosin molecule mechanics: piconewton forces and nanometre steps. *Nature* **368**, 113–118 (1994).
- Colquhoun, D. & Sigworth, F. J. in *Single-channel Recording* 2nd edn (eds Sakmann, B. & Neher, E.) 483–587 (Plenum, New York, 1995).

Acknowledgements. We thank J. Kendrick-Jones for providing the skeletal myosin S1; A. F. Huxley and M. Peckham for helpful discussions and comments; the Royal Society, British Heart Foundation, American Cancer Society and the NIH for financial support. J.D.J. held a Howard Hughes Medical Institute fellowship.

Correspondence and requests for materials should be addressed to J.E.M. (e-mail: jem1@york.ac.uk).

Structural basis for self-association and receptor recognition of human TRAF2

Young Chul Park*, Vicki Burkitt*, Anthony R. Villa*, Liang Tong† & Hao Wu*

* Department of Biochemistry, The Weill Medical College and Graduate School of Medical Sciences of Cornell University, 1300 York Avenue, New York, New York 10021, USA

† Department of Biological Sciences, Columbia University, 1212 Amsterdam Avenue, New York, New York 10027, USA

Tumour necrosis factor (TNF)-receptor-associated factors (TRAFs) form a family of cytoplasmic adapter proteins that mediate signal transduction from many members of the TNF-receptor superfamily and the interleukin-1 receptor¹. They are important in the regulation of cell survival and cell death. The carboxy-terminal region of TRAFs (the TRAF domain) is required for self-association and interaction with receptors. The domain contains a predicted coiled-coil region that is followed by a highly conserved

TRAF-C domain². Here we report the crystal structure of the TRAF domain of human TRAF2, both alone and in complex with a peptide from TNF receptor-2 (TNF-R2). The structures reveal a trimeric self-association of the TRAF domain, which we confirm by studies in solution. The TRAF-C domain forms a new, eight-stranded antiparallel β -sandwich structure. The TNF-R2 peptide binds to a conserved shallow surface depression on one TRAF-C domain and does not contact the other protomers of the trimer. The nature of the interaction indicates that an SXXE motif may be a TRAF2-binding consensus sequence. The trimeric structure of the TRAF domain provides an avidity-based explanation for the dependence of TRAF recruitment on the oligomerization of the receptors by their trimeric extracellular ligands.

To understand the molecular basis of TRAF self-association and receptor interaction, we determined the crystal structures of the TRAF domain of human TRAF2, alone and in complex with a TNF-R2 peptide (Fig. 1). We solved the structure of the peptide-free form at 2.6 Å resolution by the multiple isomorphous replacement method supplemented with six-fold non-crystallographic symmetry averaging. The refined structure at 2.2 Å resolution includes

residues 334–501 for each protomer of the two trimers in the crystal. The structure in complex with the receptor peptide (420'-QVPFSKEEC-428'; numbers marked by a prime symbol denote receptor residues), which has been shown to interact with TRAF2 (refs 2, 3), was determined by molecular replacement and refined at 2.3 Å resolution. It includes residues 311–501 for one trimer and residues 316–501 for the other trimer in the crystal. Two receptor peptides were visible for the first trimer and crystal packing contacts prevented peptide binding to the remaining four protomers, consistent with the expected low affinity of the monomeric receptor peptide. It is unlikely, however, that the observed peptide binding is a crystallographic artefact as the two copies of the peptide make essentially identical contacts with TRAF2.

Each protomer of the TRAF2 trimer contains two domains (Fig. 1). As expected from sequence analysis, the coiled-coil domain (up to residue 347) forms a single α -helix (α_N). Residues in this domain appear to be more flexible and exhibit higher average temperature factors than residues in the other domain. The TRAF-C domain, as identified from sequence analysis (residues 352–501), forms an eight-stranded antiparallel β -sandwich, with strands β_1 ,

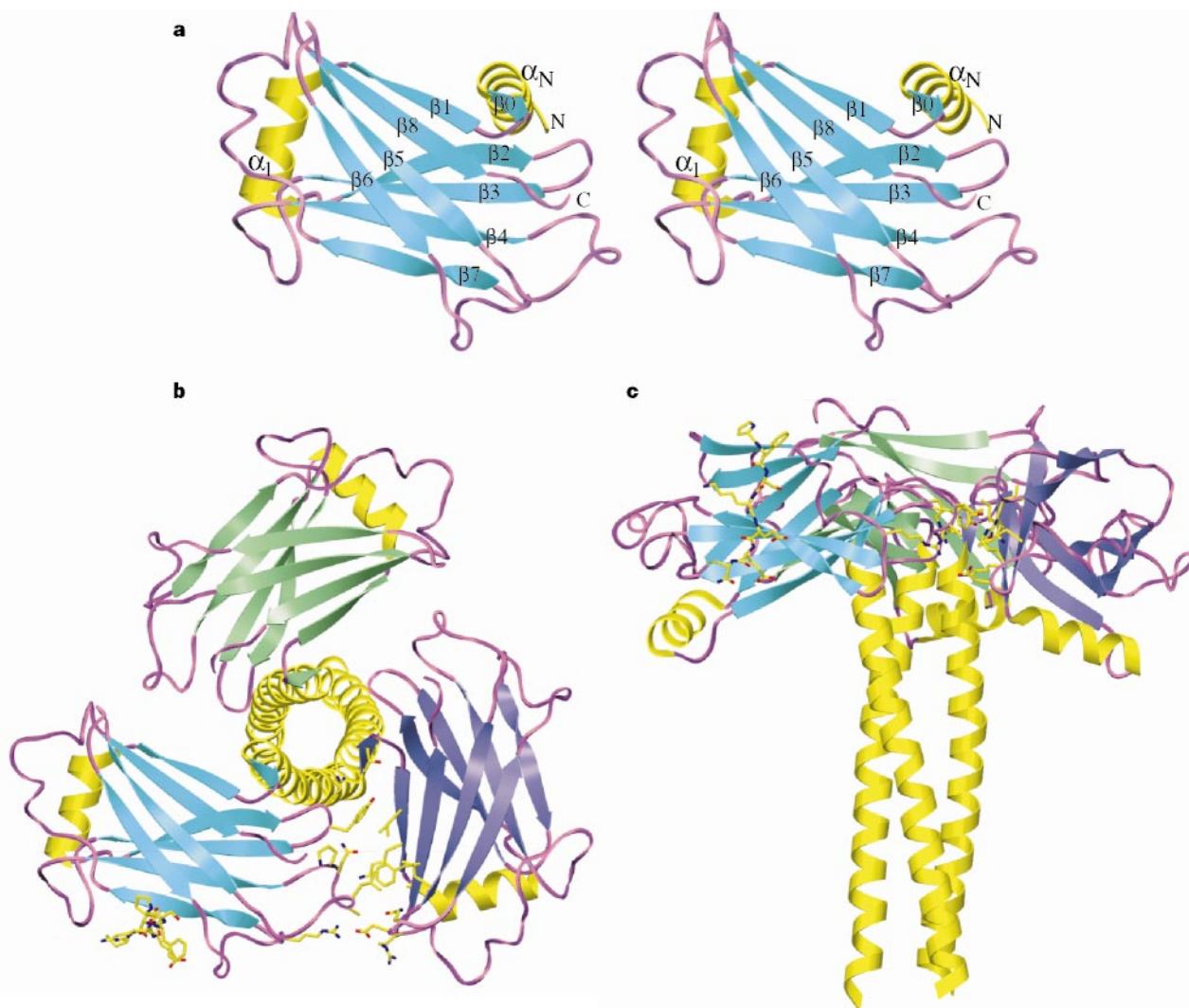


Figure 1 Structure of the TRAF domain alone and in complex with the TNF-R2 peptide. **a**, Stereo ribbon diagram of the TRAF domain of human TRAF2 in the peptide-free structure. The β -strands, α -helices and loops are shown in cyan, yellow and purple, respectively. The loop between β_7 and β_8 is highly flexible and exhibits a different conformation in the peptide-bound structure **b**, Ribbon drawing of the trimeric TRAF domain in complex with TNF-R2 peptide, looking down the three-fold axis. The β -strands in each protomer are shown in cyan,

green and dark blue. The peptide is shown as a stick model for the protomer in cyan. Residues of the TRAF-C domain in the trimer interface (between the protomers shown in cyan and dark blue) are also shown as stick models. The TRAF-C domain of the structure obeys proper three-fold symmetry, whereas the coiled-coil domain shows significant deviations. **c**, As for **b**, except that the three-fold axis is now vertical.

β 8, β 5 and β 6 in one sheet and β 2, β 3, β 4 and β 7 in the other. Strands β 2 and β 7 each contain a β -bulge, which seems to have important structural and biological functions (see below). A three-turn helix is present in the crossover connection between strands β 1 and β 2. Preceding the β -sandwich, residues 348–350 form a parallel β -structure (β 0) with strand β 2, immediately after the β -bulge in this strand. The side chains of residues in β 0 also partly cover one edge of the β -sandwich. Therefore, structural analysis suggests that residue 348 should be the start of the TRAF-C domain, even though residues 348–351 exhibit sequence variability. On the basis of visual inspection of the SCOP structure database⁴ and an automatic structural-similarity search using the Dali program⁵, the TRAF-C domain appears to represent a new fold for an eight-stranded anti-parallel β -sandwich. However, the topology observed for this domain may be reached by circular permutations of the β -strands in copper-zinc superoxide dismutase (Protein Data Bank entry 2SOD)⁶ and the C2 domain from synaptotagmin I (PDB entry Isry)⁷.

The TRAF-domain trimer has the shape of a mushroom, with the TRAF-C domain as the cap and the coiled-coil domain as the stalk (Fig. 1). The diameter of the mushroom cap ranges between 50 and 80 Å and a stalk containing five heptad repeats is 50 Å in length (residues 311–347). The parallel coiled-coil structure is formed by the hydrophobic residues at positions a and d of the heptad repeats (Fig. 2) that are characteristic of coiled-coil structures⁸. The trimer interface of the TRAF-C domain is formed by packing one end of the β -sandwich (the β 2– β 3, β 4– β 5 and β 6– β 7 connections) against an edge and a face of the β -sandwich (β 0, β 1 and β 8 strands, β 5– β 6 and β 7– β 8 connections) of the neighbouring protomer. Most residues that participate in the formation of this interface are rather hydrophobic (such as I355, Y386, A420, L421

Table 1 Receptor–TRAF2 interactions

TNF-R2	S	Area (Å ²)	VDW contacts	Potential hydrogen bonds
P422'	0.71	44	2	
F423'	0.69	73	6	
S424'	0.01	101	14	O γ : 467O γ
K425'	0.73	67	10	N: 468O; O: 468N
E426'	0.50	91	8	
E427'	0.13	139	18	N: 466O; Oe1; 395O η ; Oe1; 393N η 1; Oe2: 393N η 1 N: 399O δ 2
C428'	0.66	58	5	

S, fraction solvent accessibility of the receptor side chains; area, total surface area buried upon binding for each receptor residue; VDW contacts, number of atoms in TRAF2 that make van der Waals contacts with the receptor residue.

and F491). Hydrophilic interactions are also observed at this trimer interface, involving the side chains of K357, R385, R458 and D487. The amino-acid residues contributing to trimerization of the TRAF domain are conserved among the TRAF-family members (Fig. 2). This sequence conservation indicates that other TRAF molecules may be able to form similar homotrimers as well. Formation of heterotrimers, as has been shown for TRAF1 and TRAF2 (ref. 2), may also be possible.

The trimeric self-association of TRAF2 was confirmed by solution studies. Size characterization of a TRAF2 protein containing residues 310–501 (relative molecular mass 22,600 (M_r 22.6K)) by equilibrium ultracentrifugation showed that it is a homogeneous species of M_r 63.3K. Chemical crosslinking with glutaraldehyde produced a single band on SDS–polyacrylamide gels of approximate 65K. Similar studies in conjunction with gel-filtration analyses showed that the TRAF-domain molecule containing residues 327–501 was also trimeric. However, the TRAF domain containing residues 342–501 was monomeric. These observations indicate that the stability of the trimer may be dependent on both the coiled-coil domain and the TRAF-C domain, in agreement with earlier biological studies⁹. Structurally, each TRAF-C domain alone buries a surface area of roughly 640 Å² upon trimerization; this area is rather small compared with that produced by other stable protein–protein interactions¹⁰. The results of the solution studies indicate that a minimum of roughly three heptad repeats (residues 327–347), which produces an additional surface burial of 420 Å², may be required for trimer formation. The coiled-coil domain of TRAF4 contains only three heptad repeats, the fewest of all the TRAFs. In comparison, the coiled-coil domain of TRAF2 appears to contain up to 14 heptad repeats.

Each TNF-R2 peptide is bound symmetrically to a shallow surface depression on the side of the mushroom-shaped trimer, extending from the top to the bottom rim of the mushroom cap (Figs 1, 3). The peptide contacts only one TRAF domain, with no contacts to the other two molecules of the trimer. This mode of interaction is distinct from the interaction between TNF and the extracellular domain of its receptor; each receptor binds near the interface between neighbouring protomers in the TNF trimer¹¹. We observed no significant conformational changes near the receptor-binding sites or in the relative orientations of the protomers in the trimer upon receptor binding, although there are conformational differences in several flexible regions of the TRAF domain.

The receptor peptide assumes a nearly extended main-chain conformation in the complex (Fig. 3). The receptor-binding site in TRAF2 is formed by the exposed faces of strand β 6 in the first sheet and strands β 7, β 4 and β 3 in the second sheet. A portion of the peptide chain (K425'–E427') runs antiparallel and adjacent to the latter half of strand β 7 (residues 466–468), immediately after the β -bulge in this strand. This leads to three main-chain hydrogen bonds between the peptide and TRAF2, extending the four-stranded second β -sheet by one strand. In addition, the main-chain amide group of C428' is within hydrogen-bonding distance of the carboxylate group of D399 in TRAF2. The formation of a β -sheet has been frequently observed in protein–peptide interactions, for example in the interaction between substrates and certain serine

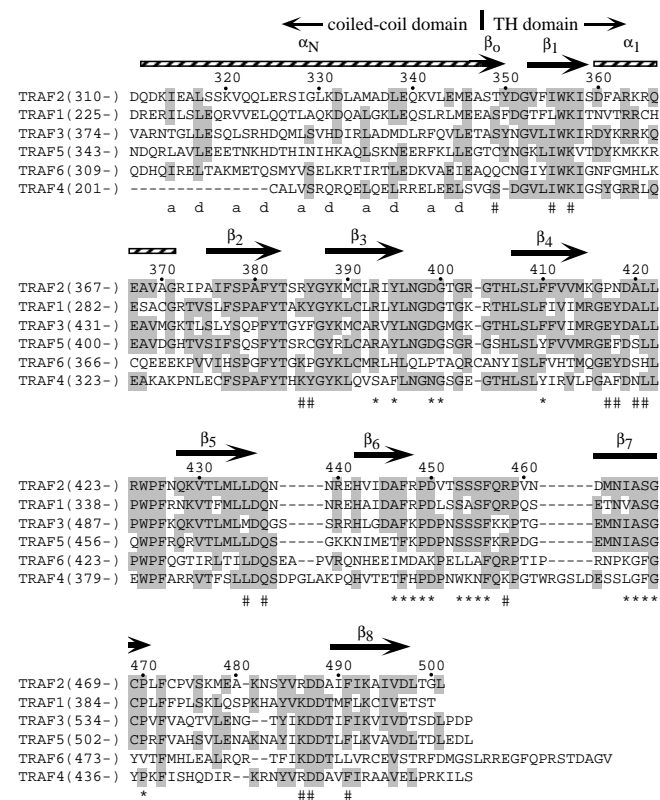


Figure 2 Structure-based sequence alignment of TRAF-family members. Secondary structures, the a and d positions of the coiled-coil domain, residues in the TRAF-C domain involved in trimerization (hash symbols), and residues interacting with the receptor peptide (asterisks) are mapped onto the TRAF2 sequence. Residues conserved among at least three TRAF family members are shaded.

proteases¹² and between peptides and the PTB and PDZ domains¹³.

Residues P422'–C428' of the receptor peptide show interactions with the TRAF2 protein (Table 1, Fig. 3), burying a surface area of 500 Å² upon binding. Residues Q420'–V421' are ordered in only one copy of the peptide, where the peptide is stabilized by crystal packing. It is likely that residues preceding P422' do not contribute to the binding. The peptide makes mostly van der Waals contacts with TRAF2, of which ~50% are polar–nonpolar contacts, 35% are nonpolar–nonpolar contacts and 15% are polar–polar contacts. Residues between F423' and C428' appear to make significant contributions to the overall binding energy, as judged by the surface area buried and the number of TRAF2 atoms in contact with these residues (Table 1). It remains to be seen whether residues following C428', which are not included in the receptor peptide used here, can also contribute to binding. Most of the receptor residues are bound to shallow pockets on the surface of the TRAF-C domain and are largely exposed to solvent, consistent with the expected low affinity of the interaction.

Residues S424' and E427' of the receptor peptide appear to be recognized specifically by TRAF2. The side chain of S424' binds to a small pocket on the surface of the protein and becomes completely buried. The hydroxyl group of S424' is within hydrogen-bonding distance of the hydroxyl group of S467 (in strand β7) of TRAF2. The side-chain carboxylate group of E427' forms an ion pair with R393 (β3), and is also hydrogen-bonded to the side-chain hydroxyl of Y395 (β3). The aliphatic portion of the E427' side chain is mainly buried, leaving 13% surface exposure for the entire side chain. It therefore appears that these two receptor residues are the major determinants of binding specificity, giving rise to an SXXE motif, where X may be one of many amino-acid residues, preferably one with a relatively large side chain. Further support for the importance of this binding motif comes from the observation that the main-chain hydrogen-bonding interactions between this peptide and TRAF2 are also mediated through these residues. They are then likely to serve as anchoring points during binding.

A homologous sequence from the receptor CD30 (residues 576–MLSVEEE–582), a member of the TNF-receptor superfamily, interacts with TRAF2 (ref. 3). The conservation of the SXXE motif in the CD30 receptor indicates that its binding to TRAF2 is likely to be the same as observed here for the TNF-R2 peptide. In agreement with our structural observations, single-point alanine mutagenesis of the CD30 peptide showed that residues L577–E581 each contributed to the overall binding energy, as assessed by co-precipitation experiments³. Further mutagenesis and quantitative binding studies are needed to determine more precisely the energetic contribution and the tolerance to mutations for each residue of the receptor peptide.

The three residues of TRAF2 (R393, Y395 and S467) that recognize the key residues in the SXXE motif of the receptor peptide are strictly conserved among TRAFs 1, 2, 3 and 5 (Fig. 2). In TRAF4, the three residues are changed to serine, phenylalanine and phenylalanine, respectively. TRAF4 appears to be localized in the nucleus¹⁴ and has not yet been shown to interact with any receptors. In TRAF6, R393 is conserved, whereas Y395 and S467 are changed to histidine and phenylalanine, respectively. The S467F change introduces a bulky phenyl ring on the surface, which may not allow the receptor peptides to bind in the same way as observed here. It is not clear from our structure why the TNF-R2 peptide binds only to TRAF1 and TRAF2, and not to TRAF3, as shown by co-precipitation experiments³. It is likely that this selectivity is caused indirectly by sequence variations outside the binding site. One such possibility is the V451P variation in TRAF3 (and in TRAFs 4–6; Fig. 2), which might change the local helical conformation observed in this structure and therefore alter the positioning of several adjacent residues involved in the peptide interaction (Fig. 3). In a similar way, adenylyl cyclase is activated by the G protein G_{sex} rather than G_{iox}, as revealed by crystallographic studies¹⁵.

TRAF proteins interact with several other linear sequences from

the intracellular domains of members of the TNF-receptor superfamily¹. For example, a PXQX(T/S) TRAF-binding motif (where X may represent any amino acid) has been identified in CD30, CD40, CD27 and LMP-1 (ref. 1). Stretches of conserved acidic residues have also been shown to mediate the binding of the receptors 4-1BB and Ox40 to TRAF molecules¹⁶. In addition, TRAF6 may bind to CD40 and the p75 neurotrophin receptor through sequences completely different from those described above^{17–19}. Whether these diverse motifs bind to the SXXE site identified here, perhaps also exploiting β-edge hydrogen bonding, or to a different TRAF site, remains to be determined by structural studies.

TRAF molecules are important mediators of signalling through

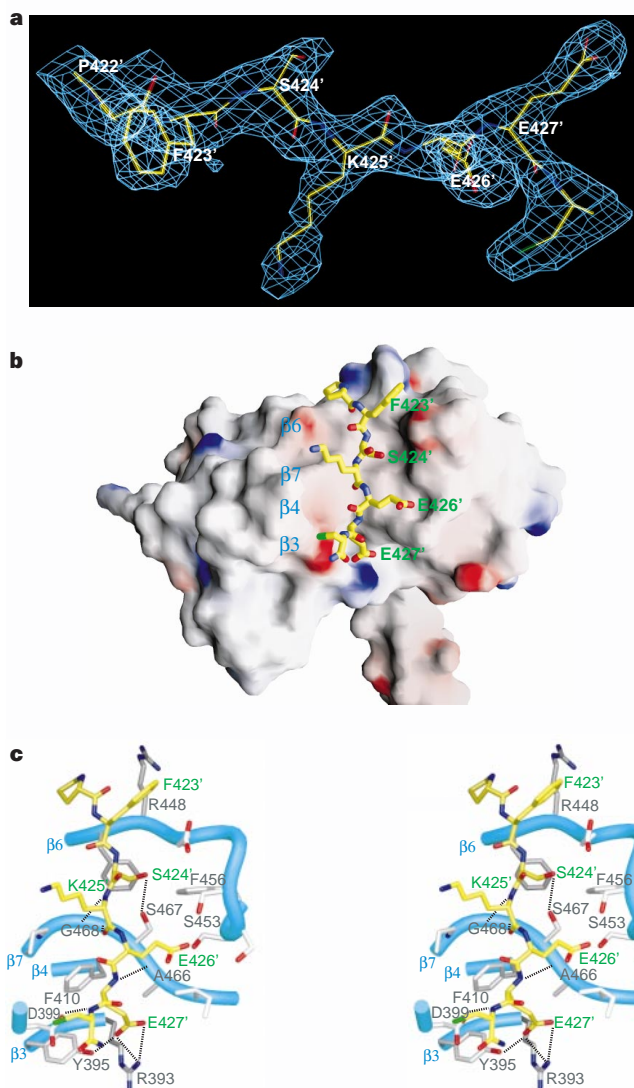


Figure 3 Detailed interaction between TRAF2 and the TNF-R2 peptide.

a, Simulated annealing omit difference map for the TNF-R2 peptide calculated with reflections between 20.0 and 2.3 Å resolution and contoured at 2.0σ. The peptide model is superimposed. **b**, Molecular surface of a TRAF2 protomer, showing the bound TNF-R2 peptide as a stick model; the three-fold axis is in the vertical orientation. Surface colour coding is according to electrostatic surface potential, scaled from –30 to +30 kTe⁻¹, with blue for positive and red for negative. Selected residues in the receptor peptide and the underlying secondary-structural elements of TRAF2 at the binding site are labelled. **c**, Stereo view of the detailed interaction between the TNF-R2 peptide (carbon atoms shown in yellow) and the TRAF2 protomer (carbon atoms shown in grey). The main chain of the TRAF2 structure is shown in cyan as backbone worms. Selected residues in the peptide (primed numbers in green) and the protein (in grey) are labelled. Hydrogen bonds and a salt bridge are shown as black dotted lines.

Table 2 Phase determination and structure refinement

Phase determination		Resolution	R_{merge}	Completeness	R_{scale}	Phasing power		
Crystal	Protein construct							
Native	327-501	40.0-2.5 Å	6.2% (26.0%)	99.0% (99.1%)				
Thimerosal (1)	327-501	40.0-2.6 Å	9.2% (31.6%)	94.9% (93.5%)	33.0%	1.9		
Thimerosal (2)	327-501	40.0-2.7 Å	7.1% (23.0%)	94.6% (92.3%)	32.8%	1.9		
Structure refinement		Resolution	R_{merge}	Completeness	Solvent atoms	Average B	R	R_{free}
Protein construct	Peptide							
327-501	No	20.0-2.2 Å	4.3% (10.7%)	99.5% (98.5%)	743	22.2 Å ²	20.9%	25.1%
310-501	Yes	20.0-2.3 Å	4.8% (27.9%)	99.0% (97.9%)	910	47.1 Å ²	23.4%	29.0%

Statistics for the last resolution shell are shown in parentheses. R_{scale} is the R-factor between native and derivative amplitudes.

members of the TNF-receptor superfamily. The extracellular events of this signalling process appear to involve the trimerization of the extracellular domains of the receptor molecules by the inherently trimeric ligands of the TNF superfamily. Ligand-induced receptor trimerization has been demonstrated by the co-crystal structure in the interaction between TNF- β and TNF-R1 (ref. 11). The significant sequence homology shared by the superfamily indicates the conservation of this extracellular interaction. The trimerization of the extracellular domains can bring the intracellular domains of the three receptor molecules into proximity, which may then be recognized optimally by the trimeric TRAF2 molecules. The avidity contribution of this oligomeric interaction is expected to increase the affinity exponentially, providing an explanation for the ligand-induced recruitment of TRAF proteins^{1,20}. In addition to direct interactions between receptors and TRAFs, TNF-R1 recruits TRAF2 indirectly through the adapter protein TRADD²¹. It remains to be demonstrated whether TRADD is also trimeric and therefore relays the avidity component of the interaction from the receptor to TRAF2.

The downstream events of TRAF-mediated signal transduction are thought to involve the activation of MAP kinases and, ultimately, transcription factors of the Rel and AP-1 family¹. This signalling process requires the amino-terminal RING and zinc-finger motifs of the TRAF molecules, although the detailed mechanisms of the process are largely unknown. Our structures show that the TRAF domain of TRAF2 may be a constitutive trimer and binds the receptor peptide without significant conformational changes. This argues against receptor-induced TRAF oligomerization or conformational change as the initiator of downstream events. However, such possibilities cannot be excluded on the basis of our data, as full-length TRAF proteins may exist in a different conformation in the unbound state. Alternatively, the recruitment of TRAFs to the cell membrane alone by the receptors might be the determining factor in the signal transduction. □

Methods

Protein preparation and crystallization. The complementary DNA encoding human TRAF2 was obtained from the library of expressed sequence tags. Two constructs of the TRAF domain of TRAF2 (residues 315-501 and residues 310-501) containing carboxy-terminal polyhistidine tags were generated using the pET24d vector (Novagen) and overexpressed in *E. coli* by induction at 20 °C. The recombinant proteins were purified by nickel-affinity chromatography (Qiagen) followed by gel filtration (Superose 12, Amersham Pharmacia). The protein containing residues 315-501 was treated with trypsin at 4 °C for 2 h at a 1:1,000 molar ratio, which removed residues 315-326. The digested protein was further purified and then crystallized at 20 °C from a solution containing 11% PEG4000 and 0.1 M MES, pH 6.0. The crystals belong to space group C2 with cell dimensions of $a = 134.9 \text{ \AA}$, $b = 85.0 \text{ \AA}$, $c = 124.1 \text{ \AA}$ and $\beta = 118.6^\circ$. The protein containing residues 310-501 was crystallized from 12% PEG4000 0.2 M ammonium acetate, and 0.1 M citrate, pH 5.6, in the presence of an equal molar concentration (1 mM) of the peptide from TNF-R2 (residues 420'-QVPSKEEC-428'). The peptide was chemically synthesized with N-terminal acetylation and C-terminal amidation to mimic the intact protein. The estimated K_d of the interaction (0.1-1.0 mM; preliminary results) indicates that the binding sites may not be fully saturated under these crystallization conditions. Although similar crystals can be obtained in the absence of the peptide, higher concentrations of the peptide prevented crystal growth,

indicating competition with crystal packing. The crystals belong to space group $P2_1$ with cell dimensions of $a = 83.0 \text{ \AA}$, $b = 84.4 \text{ \AA}$, $c = 100.7 \text{ \AA}$ and $\beta = 108.7^\circ$. Both crystal forms contain two trimers of the TRAF2 protein per crystallographic asymmetric unit.

Structure determination and analysis. All X-ray diffraction data (Table 2) were collected on cryoprotected crystals and processed with the HKL package²². Native and derivative data for the peptide-free crystals were measured on an R-axis IV imaging plate system mounted on a Rigaku RU300 rotating anode X-ray generator. Heavy-atom positions were located from the isomorphous differences by direct methods using SHELX²³; some of these positions were also found by Patterson interpretation using PATSOL²⁴. MIR phases were calculated for reflections up to 2.6 Å resolution with the program PHASES²⁵. After solvent-flattening, the phases were further improved by six-fold non-crystallographic symmetry (NCS) averaging with a locally written program (L.T., unpublished results). Sequence fitting and model building were done with program O (ref. 26). A 2.2 Å data set collected using the CCD detector at the CHESS F2 beamline was used for the crystallographic refinement, with the program CNS²⁷. NCS restraints were used throughout the refinement. Diffraction data of the peptide complex were collected at the X4A beamline of NSLS. The structure was determined by molecular-replacement calculations with the program REPLACE²⁸ using the trimer atomic model from the peptide-free structure and refined at 2.3 Å resolution using program CNS²⁷. An $|F_o| - |F_c|$ difference map clearly showed the electron densities for the bound peptides and for the extra N-terminal residues. The coiled-coil region of the protein deviates from non-crystallographic symmetry and NCS restraints were applied to the TRAF-C domain alone. Molecular surface representations and stick models were produced with the program GRASP²⁹ and ribbon diagrams were generated using the program SETOR³⁰.

Characterization of oligomerization in solution. Equilibrium sedimentation was done at 20 °C on protein samples at 25 μM concentration using an XL-A Optima analytical ultracentrifuge (Beckman) running at 11,000 r.p.m. Data were fit to a single species model. The apparent relative molecular mass was calculated by assuming a partial specific volume of 0.74 ml g⁻¹ and a solvent density of 1.045 g ml⁻¹. Chemical crosslinking was done at room temperature with 5 μM protein samples in the presence of an 8,000-fold molar excess of glutaraldehyde. The reaction mixtures were quenched with excess glycine after 40-min incubations, concentrated using Microcons (Amicon) and separated by SDS-PAGE.

Received 18 January; accepted 24 February 1999.

1. Arch, R. H., Gedrich, R. W. & Thompson, C. B. Tumor necrosis factor receptor-associated factors (TRAFs)—a family of adapter proteins that regulates life and death. *Genes Dev.* **12**, 2821-2830 (1998).
2. Rothe, M., Wong, S. C., Henzel, W. J. & Goeddel, D. V. A novel family of putative signal transducers associated with the cytoplasmic domain of the 75 kDa tumor necrosis factor receptor. *Cell* **78**, 681-692 (1994).
3. Boucher, L., Marengere, L. E. M., Lu, Y., Thukral, S. & Mak, T. W. Binding sites of cytoplasmic effectors TRAF1, 2, and 3 on CD30 and other members of the TNF receptor superfamily. *Biochem. Biophys. Res. Commun.* **233**, 592-600 (1997).
4. Murzin, A. G., Brenner, S. E., Hubbard, T. & Chothia, C. SCOP: a structural classification of protein database for the investigation of sequences and structures. *J. Mol. Biol.* **247**, 536-540 (1995).
5. Holm, L. & Sander, C. Dali: a network tool for protein structure comparison. *Trends Biochem. Sci.* **20**, 478-480 (1995).
6. Tainer, J. A., Getzoff, E. D., Beem, K. M., Richardson, J. S. & Richardson, D. C. Determination and analysis of the 2 Å-structure of copper, zinc superoxide dismutase. *J. Mol. Biol.* **160**, 181-217 (1982).
7. Sutton, R. B., Davletov, B. A., Berghuis, A. M., Sudhof, T. C. & Sprang, S. R. Structure of the first C2 domain of synaptotagmin I: a novel Ca²⁺/phospholipid-binding fold. *Cell* **80**, 929-938 (1995).
8. Harbury, P. B., Zhang, T., Kim, P. S. & Alber, T. A switch between two-, three-, and four-stranded coiled coil in GCN4 leucine zipper mutants. *Science* **262**, 1401-1407 (1993).
9. Takeuchi, M., Rothe, M. & Goeddel, D. V. Anatomy of TRAF2. *J. Biol. Chem.* **271**, 19935-19942 (1996).
10. Janin, J., Miller, S. & Chothia, C. Surface, subunit interfaces and interior of oligomeric proteins. *J. Mol. Biol.* **204**, 155-164 (1988).

11. Banner, D. W. *et al.* Crystal structure of the soluble human 55 kd TNF receptor-human TNF beta complex: implications for TNF receptor activation. *Cell* **73**, 431–445 (1993).
12. Tong, L. *et al.* Conserved mode of peptidomimetic inhibition and substrate recognition of human cytomegalovirus protease. *Nature Struct. Biol.* **5**, 819–826 (1998).
13. Kuriyan, J. & Cowburn, D. Modular peptide recognition domains in eukaryotic signaling. *Annu. Rev. Biophys. Biomol. Struct.* **26**, 259–288 (1997).
14. Regnier, C. H. *et al.* Presence of a new conserved domain in CART1, a novel member of the tumor necrosis factor receptor-associated protein family, which is expressed in breast carcinoma. *J. Biol. Chem.* **270**, 25715–25721 (1995).
15. Sunahara, R. K., Tesmer, J. J. G., Gilman, A. G. & Sprang, S. R. Crystal structure of the adenylyl cyclase activator Gsa. *Science* **278**, 1943–1947 (1997).
16. Arch, R. H. & Thompson, C. B. 4-1BB and Ox40 are members of a tumor necrosis factor (TNF)-nerve growth factor receptor subfamily that bind TNF receptor-associated factors and activate nuclear factor κ B. *Mol. Cell Biol.* **18**, 558–565 (1998).
17. Ishida, T. *et al.* Identification of TRAF6, a novel tumor necrosis factor receptor-associated factor protein that mediates signaling from an amino-terminal domain of the CD40 cytoplasmic region. *J. Biol. Chem.* **271**, 28745–28748 (1996).
18. Pullen, S. S. *et al.* CD40-tumor necrosis factor receptor-associated factor (TRAF) interactions: regulation of CD40 signaling through multiple TRAF binding sites and TRAF hetero-oligomerization. *Biochemistry* **37**, 11836–11845 (1998).
19. Khursigara, G., Orlinick, J. R. & Chao, M. V. Association of tumor necrosis factor receptor-associated protein 6 (TRAF6) with the p75 neurotrophin receptor. *J. Biol. Chem.* **274**, 2597–2600 (1999).
20. Kuhne, M. R. *et al.* Assembly and regulation of the CD40 receptor complex in human B cells. *J. Exp. Med.* **186**, 337–342 (1997).
21. Hsu, H., Shu, H.-B., Pan, M.-G. & Goeddel, D. V. TRADD-TRAF2 and TRADD-FADD interactions define two distinct TNF receptor 1 signal transduction pathways. *Cell* **84**, 299–308 (1996).
22. Otwinowski, Z. & Minor, W. Processing of X-ray diffraction data collected in oscillation mode. *Methods Enzymol.* **276**, 307–326 (1997).
23. Sheldrick, G. M. Phase annealing in SHELX-90: direct methods for larger structures. *Acta Crystallogr. A* **46**, 467–473 (1990).
24. Tong, L. & Rossmann, M. G. Patterson-map interpretation with noncrystallographic symmetry. *J. Appl. Crystallogr.* **26**, 15–21 (1993).
25. Furey, W. Phases: a program package for the processing and analysis of diffraction data for macromolecules (VA Medical Center, Pittsburgh, 1993).
26. Jones, T. A., Zou, J.-Y., Cowan, S. W. & Kjeldgaard, M. Improved methods for building models in electron density maps and the location of errors in those models. *Acta Crystallogr. A* **47**, 110–119 (1991).
27. Brunger, A. T. *et al.* Crystallography & NMR system: a new software suite for macromolecular structure determination. *Acta Crystallogr. D* **54**, 905–921 (1998).
28. Tong, L. REPLACE, a suite of computer programs for molecular-replacement calculations. *J. Appl. Crystallogr.* **26**, 748–751 (1993).
29. Nicholls, A., Sharp, K. A. & Honig, B. Protein folding and association: insights from the interfacial and thermodynamic properties of hydrocarbons. *Proteins* **11**, 281–296 (1991).
30. Evans, S. V. SETOR: hardware-lighted three-dimensional solid model representations of macromolecules. *J. Mol. Graph.* **11**, 134–138 (1993).

Acknowledgements. We thank W. Hendrickson for discussions; T. Burling for maintaining the X-ray equipment and computers; C. Ogata for assistance at the X4A beamline of NSLS; members of the CHES for help at the F2 beamline; M. Lu for running the analytical ultracentrifugation experiments; C. Lima for help with the SETOR program; and G. Douglas and M. Cervantes for summer research in the laboratory.

Correspondence and requests for materials should be addressed to H.W. (e-mail: haowu@mail.med.cornell.edu). Atomic coordinates have been deposited in the Brookhaven Protein Data Bank under accession numbers 1ca4 and 1ca9.